การประชุมวิชาการเครือข่ายวิศวกรรมเครื่องกลแห่งประเทศไทยครั้งที่ 17
15-17 ตุลาคม 2546 จังหวัดปราจีนบุรี

Flow Visualization of Secondary Flow near Blade/Endwall Region in a Linear Turbine Cascade

Surachai Sanitjai*
Department of Mechanical Engineering, Faculty of Engineering, King Mongkut's University of Technology Thonburi
91 Pracha-u-tid Rd. Bangmod Tungkru Bangkok 10140 Thailand
Tel: 0-24709117 Fax: 0-24709111 E-mail: surachai.san@kmutt.ac.th

Abstract

A visualization of the flow on endwall, suction and pressure surfaces of the linear turbine blades is performed to investigate the secondary flow near the blade/endwall region. Effect of upstream component misalignment on the secondary flow is also studied. An oil-lampblack technique is used. Photographs of the flow pattern for the cases of flat endwall, forward- and backward-facing step show a complex vortex system. On the endwall, traces of a suction side leading edge corner vortex, suction side corner vortex, passage vortex and pressure side leg of horseshoe vortex are observed. On the suction surface, traces of a suction side leg of horseshoe vortex, passage vortex, wall vortex induced by the passage vortex, and suction side corner vortex are found. Results of the flow visualization are compared to heat/mass transfer results and found to be in a good agreement.

1. Introduction

An approaching flow in a gas turbine passage is complex and characterized by high turbulence and periodic variations due to vortices and wakes shed from upstream stages. Additionally, separated flow regions, boundary layer transition and high flow acceleration can take place because the passage is curved. The secondary vortex flows near a blade/endwall region add more sophisticated features to the complexity of an effective design of a modern gas turbine engine.

Flow visualization is useful in understanding the secondary vortex flows, and their effects on blade heat transfer. In addition the secondary flows produced close to an endwall cause an extra pressure loss and increase the rate of heat transfer on both the endwall and the blade surface near the junction of endwall and blades.

The aerodynamic performance of a turbine and increase in heat transfer rate from the hot fluid to the surfaces of the blade and endwall may be significantly affected by flow separation, a horseshoe vortex, a passage vortex and some small but very intense corner vortices at the junction of endwall and blade of a turbine cascade. A comprehensive review of the secondary flow structures in turbine cascades has been presented by Sieverding [1]. Detailed experimental information about secondary flow visualization and the secondary flow patterns can be found in [2-9].

Langston et al. [7] observed that the passage vortex originated near the pressure side of the blade and increased in size through the passage, entraining fluid from both the mainstream and the separated fluid from the endwall and suction surface boundary layers.

To assist in visualizing the flow patterns and to aid in understanding this complicated flow, several secondary flow models have been proposed. The vortex flow pattern by [10-12] suggests that the suction leg wraps itself around the passage vortex instead of adhering to the suction surface. Goldstein and Spores [12] proposed that the suction leg of the horseshoe vortex stays above the passage vortex and travels with it. Among the three models, the location of the suction leg of the horseshoe vortex is the major difference. The suction leg, as it moves down the passage, is difficult to follow. Most pressure or velocity maps in the literature do not give a clear picture of how this leg develops. Its small size combined with a strong stretching in the streamwise direction makes it difficult to detect. Moore and Smith [13] and Sieverding and VandenBosche [14] found that the suction side leg wraps around the passage vortex.

Sonoda [6] found a new vortex pair which moves above the passage vortex and stays close to the suction surface. Jabbari et al. [2] observed in their surface flow visualization that this new vortex is essentially a part of an endwall corner vortex which climbs up the suction surface by the up-wash of the passage vortex.

The secondary flow greatly affects the heat transfer on the endwall and blade suction surfaces, but not on the pressure surface [15-16]. Near the endwall the local heat transfer enhancement was about 60% greater than the mid-span value [16]. The average heat transfer rate on an endwall was almost doubled downstream of the linear turbine cascade and local heat transfer enhancement of more than five times was detected [12], indicating a strong influence of the secondary flow.

In this paper, flow development in a linear cascade is examined for low freestream turbulence and a turbulent boundary layer on the endwall. Comparisons are made to the mass transfer distribution on both the pressure and suction surfaces of the blade.

Since the endwall of a turbine blade is not made up of one continuous piece, there is a gap at the interface between the rotor and stator components. Leakage flow through the gap is supplied in order to cool the interface and prevent ingestion of hot gases into the gap. Additionally, component misalignment occurs because of casting, manufacturing, assembly, maintenance, and thermal growth. The effect of upstream component misalignment is also investigated in this study by introducing an upstream slot in front of the turbine blade cascade.

2. Experimental Apparatus

2.1 Wind tunnel and test section

The wind tunnel used for the flow visualization is a multi-purpose blowing type wind tunnel. Air flows through a heat exchanger before entering a couple of settling chambers. The air flow is guided through a squared contraction nozzle with an area ratio of 6.25. The exit of the contraction has the dimension of 45.7 x 45.7 cm^2. The exit velocity at the contraction without the test section connected is about 40 m/s while the turbulence level is about 0.2%. A small trip wire is placed on the bottom endwall at the exit of the contraction to make the turbulent boundary layer flow more uniform.

The test section, shown in Fig. 1, is connected to the wind tunnel contraction. All the walls of the test section are made of 1.9cm thick Plexiglas. The cascade is a five blade setup plus two bypass flexible walls. The two tailboards behind the two outside blades and the flexible walls can be adjusted while monitoring the static pressure to balance the flow distribution in the central passage with the neighboring passages in order to get uniform flows in each passage. Several slots are cut into the walls ahead of and behind the cascade to insert probes to measure pressure, velocity and temperature. The cascade geometries are shown in Fig. 2. The cascade and test-section data and the flow conditions are listed in Table 1.

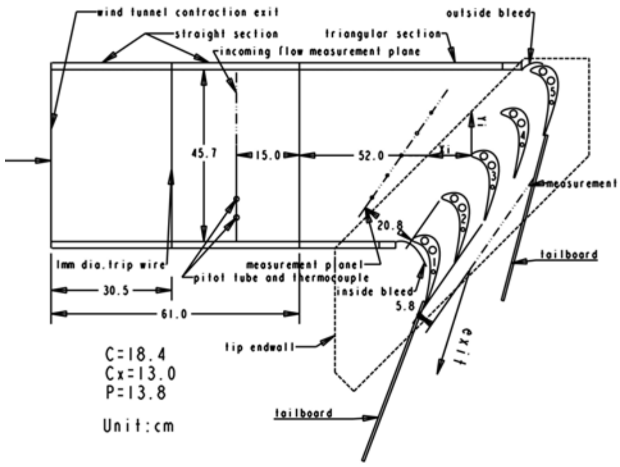

Fig. 1 Wind tunnel test section

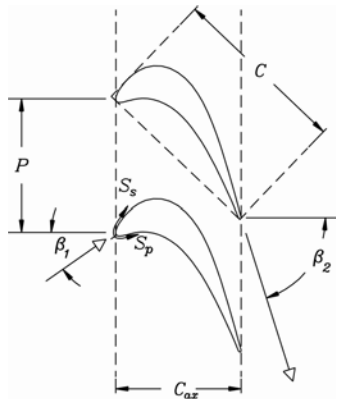

Fig. 2 Turbine blade geometry

2.2 Flow balancing

A pressure blade is used to measure the static pressure distribution on the pressure and suction surfaces of the turbine blade to check if the flow through the passage is uniform. It is a hollowed-out aluminum blade with 25 pressure taps. The static pressure distribution is measured at midspan of the blade. The balanced flow through the passages is achieved when the static pressure distribution matches the potential flow calculation. The results of static pressure distribution measured along the suction and pressure surface is shown in Fig. 3. The solid lines in the figure are the results calculated from potential flow theory. The static pressure data match quite well with the calculation.

2.3 Upstream component misalignment

The effect of upstream component misalignment on fluid flow is studied by introducing an upstream slot in front of the turbine blade cascade. A schematic diagram of misalignment configurations is shown in Fig. 4. Three misalignment configurations, i.e. flat surface, forward-facing step and backward-facing step, are used. In this study, the slot has 4 mm width, 45° angle, and 25.5 mm length. Distance from the slot to leading edge of the turbine cascade is 13 mm. For the cases of forward and backward-facing step, a step height is 4 mm.

Table 1. Cascade and Test Section Data

Number of blades	5
Chord length of blade (C)	18.42 cm
Axial chord of blade (C_x)	12.97 cm
Pitch of cascade (P)	13.81 cm
Height of cascade (H)	45.7 cm
Blade inlet angle (β_1)	35^o
Blade outlet angle (β_2)	-72.49^o
Inlet/Exit area ratio of the cascade	2.72
Exit Reynolds number – $Re_{ex}x10^{-5}$ range	4.5-6.9

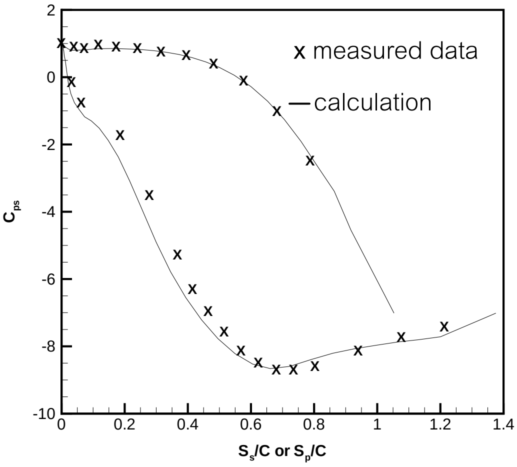

Fig. 3 Static pressure distribution

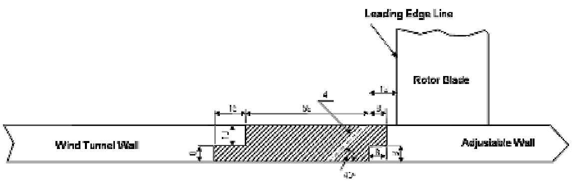

(a) flat endwall

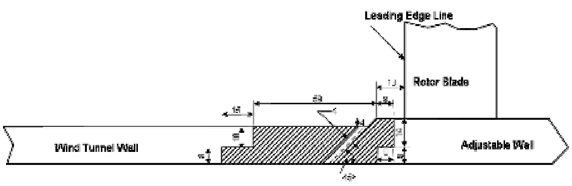

(b) endwall with forward-facing step

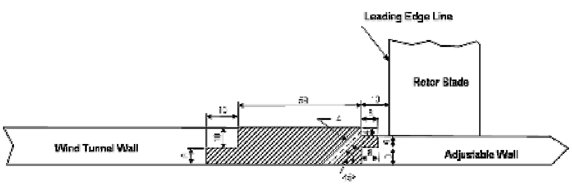

(c) endwall with backward-facing step

Fig 4. Schematic diagram of gap configurations

3. Experimental Technique

Flow visualization on the endwall, pressure and suction surfaces of the linear turbine blade is conducted using an oil-lampblack technique. A mixture of fine lampblack and light oil is spread thinly over a thin sheet of contact paper smoothly attached to the endwall, suction and pressure surfaces of the turbine blade. As the flow passes over the surfaces, the oil mixture follows the flow direction at the surfaces. The shear flow near the wall drives the particles through the oil, leaving streaks which give an indication of the local shear stress. In addition, regions of higher and lower shear can be identified by comparing the relative amount of oil mixture flow on the surfaces.

The flow visualization measurements presented are conducted within the central passage of the cascade. The exit Reynolds number for the tests is about $5.2x10^5$ and the running time is about 25 minutes.

4. Results and Discussion

4.1 Endwall flow

Flow visualization pictures on the endwall are shown in Fig. 5 for the cases of a flat endwall, forward- and backward-facing step. A flow pattern is consistent with a flow model presented in Fig. 10. The surface flow pattern on the endwall for the case of flat endwall without cavity in Fig. 5a shows traces of a suction side leading edge corner vortex (V_{sLc}), suction side corner vortex (V_{sc}), passage vortex (V_p), pressure side leg of horseshoe vortex (V_{ph}). The pressure-side horseshoe vortex (V_{ph}) moves toward the suction side of the adjacent blade. Between the adjacent blades, fluid in the endwall boundary layer flows in a converging region toward the suction surface of the blade due to the pressure gradient.

The boundary layer fluid is swept up into the passage vortex as it approaches the merge point. Thus, the crossflow in the passage can be interpreted as feeding these legs of the horseshoe vortex system and is responsible for some of the growth of the vortex system.

Downstream of the merge point, the black powder has been completely removed from the surface. This could be due to the counter rotating of the passage vortex and the accumulation of oil in this region.

For the case of flat endwall with cavity, Fig. 5b, those four vortices (V_{sLc}, V_{sc}, V_p and V_{ph}) are present and there is another additional trace of vortex (V_i) at the middle of the passage. For the case of forward-facing step, Fig. 5c, V_{sLc}, V_{sc}, V_p and V_{ph} can be seen, but it is not clear that V_i exits due to an accelerated flow in the endwall boundary layer. For the case of backward facing step, Fig. 5d, a trace of V_{sc} is not clear due to separation and reattachment downstream of the backward-facing step. However, a trace of V_i can be clearly observed. Further study for the development of V_i is necessary.

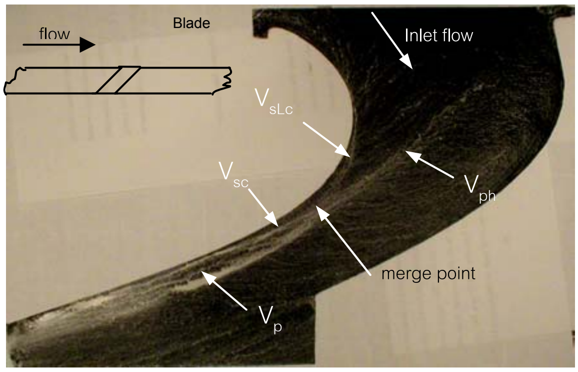

(a) Flat endwall without slot

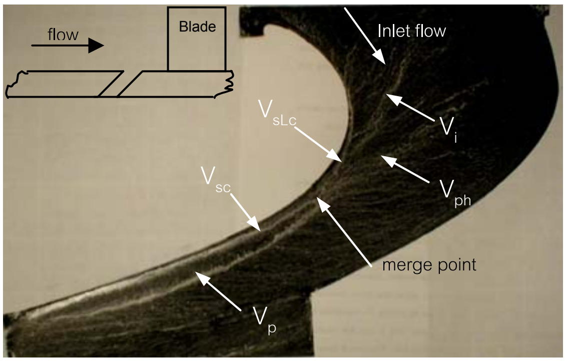

(b) Flat endwall with cavity

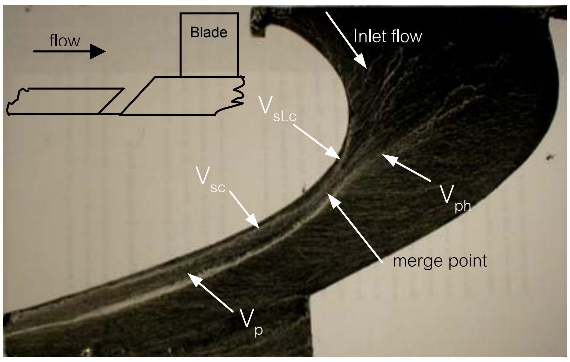

(c) Endwall with forward-facing step

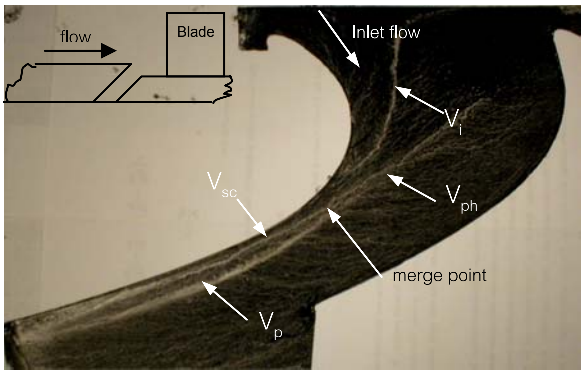

(d) Endwall with forward-facing step

Fig. 5 Visualization pictures on the endwall

4.2 Suction side flow

Photographs of flow pattern on the blade suction surface are presented in Fig. 6 for the cases of flat endwall, forward- and backward-facing step. In Fig. 6a for the case of flat endwall, traces of a suction side leg of horseshoe vortex (V_{sh}), passage vortex (V_p), wall vortex induced by the passage vortex (V_{wip}), and suction side corner vortex (V_{sc}) are found. The path of the passage vortex moves away from the endwall after the merge point. Generally, the flow pattern agrees well with the model in Fig. 10.

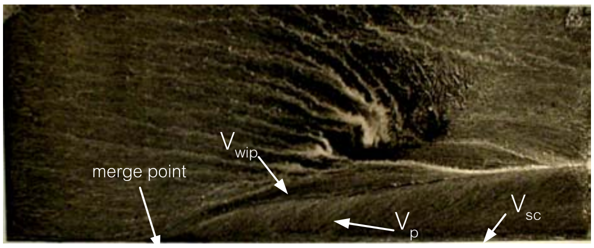

(a) flat endwall

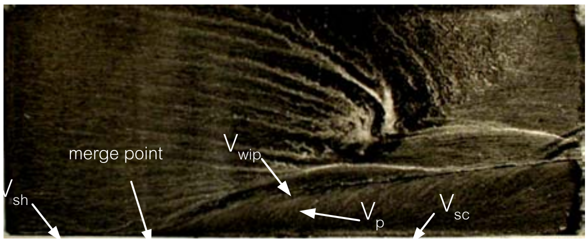

(b) endwall with forward-facing step

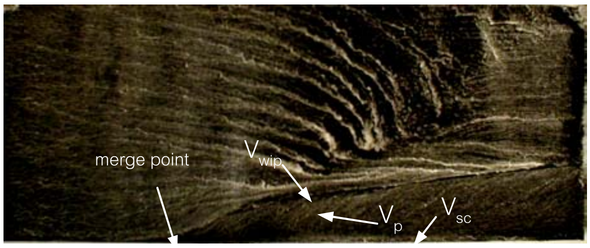

(c) endwall with backward-facing step

Fig. 6 Visualization pictures on the suction surface

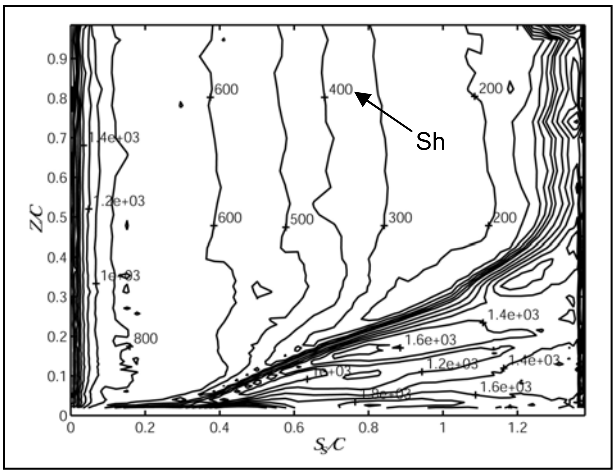

Fig. 7 Mass transfer on the suction surface (from [17])

For the case of forward-facing step, Fig. 6b, all four vortices (V_{sh}, V_p, V_{wip} and V_{sc}) are still present but V_{wip} moves closer to the endwall. For the case of backward-facing step, Fig. 6c, a trace of V_{sh} is not observed. V_{wip} moves closer to the endwall and possibly merges with the passage vortex.

Both the passage and wall induced vortex paths correspond to the two peaks in the mass transfer Sherwood number (Sh) shown in Fig. 7. High mass transfer rate in the triangular region is caused by the passage vortex. Above the triangular region on the surface, it appears that the flow in Fig. 6 moves toward the endwall. The downward direction in the oil flow visualization is caused by gravity. Mass transfer result in Fig. 7 indicates that the flow above the triangle region is two-dimensional.

4.3 Pressure side flow

A flow visualization picture on the pressure surface is shown in Fig. 8 for the case of flat endwall. Similar flow patterns are observed for the cases of forward- and backward-facing step (pictures not shown). Effect of upstream misalignment (forward- and backward- step) on flow near pressure surface is comparatively small. The separation bubble and reattachment line are not distinct. The black area and downward motion by the oil mixture indicate a very low shear region.

The contour of the mass transfer Sherwood number (Sh) shown in Fig. 9 confirms the flow separation after the inflection point and near the endwall.

Fig. 8 Visualization picture on the pressure surface

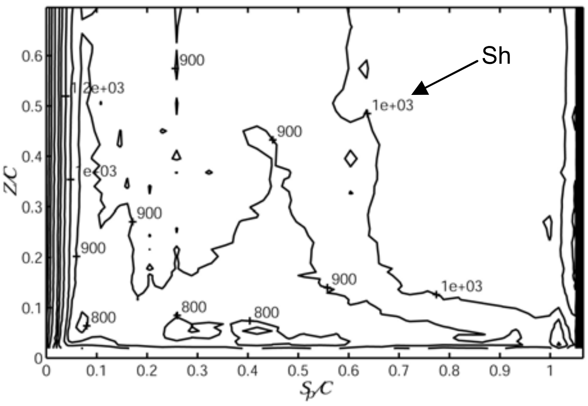

Fig. 9 Mass transfer on the pressure surface (from [17])

4.4 Model of the Secondary Flow

As shown in Fig. 10, when the horseshoe vortex is formed around the leading edge of a blade, its size is very small, similar to the size of the boundary layer thickness. During its crossflow to the suction side, the pressure leg (V_{ph}) is gradually entrained by the fluid from the boundary layer, crossflow and main flow to form a much more vigorous passage vortex whereas the suction leg (V_{sLc}) essentially maintains the same size as it wraps itself around the passage vortex traveling downstream. The multi-vortex structure of the horseshoe vortex system becomes a single vortex system after the merge point as the flow moves downstream. A suction side corner vortex (V_{sc}) is induced by the passage vortex. There are some small vortices (V_{wip}) which wrap themselves around the passage vortex as counter rotating partners to the passage vortex.

The suction surface and the endwall are most affected by the secondary flows because they are the main bounding walls of the passage vortex. It can be expected that there is a large pressure drop and higher heat transfer rate to the suction and endwall surfaces due to the strong three-dimensional flow.

For the flat endwall without a cavity, flow visualization result is similar to the model described by Wang [17]. However, for the cases of flat endwall with a cavity and backward-facing step, there is a new induced vortex (V_i) shown in Fig. 10 in the middle of passage. Additionally, for the case of backward-facing step, V_{sc} may be diminished. Effect of component misalignment strongly influences the flow structure in the region near the blade/endwall junction.

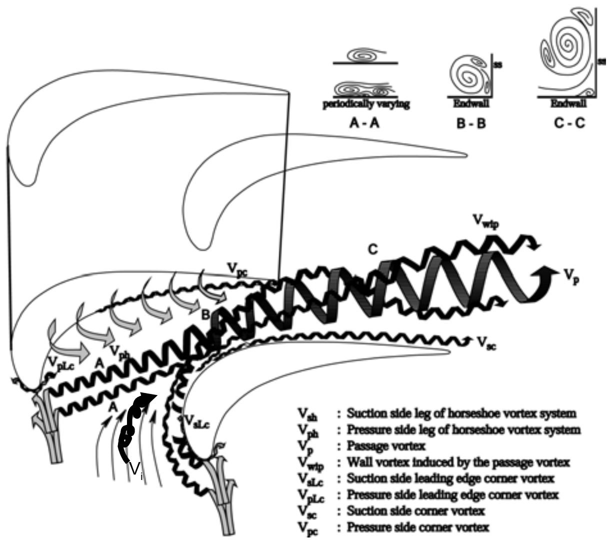

Fig. 10 Vortex flow pattern (adopted from [17])

5. Summary and Conclusion

The surface flow visualizations using pigment-oil mixtures have been conducted to view the secondary flow pattern near the endwall in the linear turbine blade cascade. Effects of component misalignment on the pattern of secondary flow are also investigated. From the flow visualization results the conclusion can be summarized as follow:

(1) For the flat endwall without a cavity, the flow patterns on the endwall, suction and pressure surfaces are similar to the model described by Wang [17].

(2) A wall vortex induced by the strong passage vortex (V_{wip}) is strongly affected by the component misalignment. It moves closer to the endwall for the cases of forward- and backward-facing step.

(3) Flow visualization results on the pressure surface indicate that the effect of component misalignment is small compared to the one on suction surface.

(4) A new induced vortex (V_i) is found in the passage flow for the cases of a flat endwall with cavity and backward-facing step.

6. References

[1] C. H. Sieverding "Recent Progress in the Understanding of Basic Aspects of Secondary Flows in Turbine Blade Passages", Journal of Engineering for Gas Turbines and Power, 1985, Vol. 107, pp. 248-257

[2] M. Y. Jabbari, Goldstein R. J., Marston K. C. and Eckert E. R. G. "Three Dimensional Flow at the Junction Between a Turbine Blade and Endwall", Wärme- und Stoffübertragung, 1992, Vol. 27, pp. 51-59

[3] L. S. Langston "Research on Cascade Secondary and Tip-Leakage Flows-Periodicity and Surface Flow Visualization, AGARD-CP-390, Secondary Flows in Turbomachines, 1990, pp. 5.1-5.6

[4] A. Yamamoto "Production and Development of Secondary Flows and Losses in Two Types of Straight Turbine Cascades: Part 1- Stator Case", Journal of Turbomachinery, 1987, Vol. 109, pp. 186-193

[5] A. Yamamoto "Production and Development of Secondary Flows and Losses in Two Types of Straight Turbine Cascades: Part 2 - Rotor Case", Journal of Turbomachinery, 1987, Vol. 109, pp. 194-200

[6] T. Sonoda "Experimental Investigation on Spatial Development of Streamwise Vortices in a Turbine Inlet Guide Vane Cascade", ASME Paper 85-GT-20, 1985

[7] L. S. Langston, Nice M. L. and Hopper R. M. "Three-Dimensional Flow Within a Turbine Cascade Passage", Journal of Engineering for Power, 1977, Vol. 99, pp. 21-28

[8] P. H. Marchal and Sieverding C. H. *Secondary Flows Within Turbomachinery Bladings*, AGARD-CP-214, Secondary Flows in Turbomachines, 1977

[9] J. T. Chung and Simon T. W. "Effectiveness of the Gas Turbine Endwall Fences in Secondary Flow Control at Elevated Freestream Turbulence Levels", ASME Paper 93-GT-51, 1993

[10] L. S. Langston "Crossflows in a Turbine Cascade Passage", Journal of Engineering for Power, 1980, Vol. 102, pp. 866-874

[11] O. P. Sharma and Butler T. L. "Predictions of Endwall Losses and Secondary Flows in Axial Flow Turbine Cascades", Journal of Turbomachinery, 1987, Vol. 109, pp. 229-236

[12] R. J. Goldstein and Spores R. A. "Turbulent Transport on the Endwall in the Region Between Adjacent Turbine Blades", Journal of Heat Transfer, 1988, Vol. 110, pp. 862-869

[13] J. Moore and Smith B. L. "Flow in a Turbine Cascade: Part2-Measurements of Flow Trajectories by Ethylene Detection", Journal of Engineering for Gas Turbines and Power, 1984, Vol. 106, pp. 409-413

[14] C. H. Sieverding and VandenBosche P. "The Use of Coloured Smoke to Visualize Secondary Flows in a Turbine-Blade Cascade", Journal of Fluid Mechanics, 1983, Vol. 134, pp. 85-89

[15] R. A. Graziani, Blair M. F., Taylor J. R. and Mayle R. E. "An Experimental Study of Endwall and Airfoil Surface Heat Transfer in a Large Scale Turbine Blade Cascade", Journal of Engineering for Power, 1980, Vol. 102, pp. 257-267

[16] M. F. Blair "An Experimental Study of Heat Transfer in a Large-Scale Turbine Rotor Passage", Journal of Turbomachinery, 1994, Vol. 116, pp. 1-13

[17] H. P. Wang "Local Mass Transfer Measurement from a Turbine Blade: Influence of High Turbulence with Large Length Scale on Heat/Mass Transfer", 1997, Ph.D. Thesis, Department of Mechanical Engineering, University of Minnesota